◆ Human Brain Mapping 30:3127–3141 (2009) ◆

Functionally Linked Resting-State Networks Reflect the Underlying Structural Connectivity Architecture of the Human Brain

Martijn P. van den Heuvel,* René C.W. Mandl, René S. Kahn, and Hilleke E. Hulshoff Pol

Rudolf Magnus Institute of Neuroscience, University Medical Center, Utrecht, The Netherlands

Abstract: During rest, multiple cortical brain regions are functionally linked forming *resting-state networks*. This high level of functional connectivity within resting-state networks suggests the existence of direct neuroanatomical connections between these functionally linked brain regions to facilitate the ongoing interregional neuronal communication. White matter tracts are the structural highways of our brain, enabling information to travel quickly from one brain region to another region. In this study, we examined both the functional and structural connections of the human brain in a group of 26 healthy subjects, combining 3 Tesla resting-state functional magnetic resonance imaging time-series with diffusion tensor imaging scans. Nine consistently found functionally linked resting-state networks were retrieved from the resting-state data. The diffusion tensor imaging scans were used to reconstruct the white matter pathways between the functionally linked brain areas of these resting-state networks. Our results show that well-known anatomical white matter tracts interconnect at least eight of the nine commonly found resting-state networks, including the default mode network, the core network, primary motor and visual network, and two lateralized parietal-frontal networks. Our results suggest that the functionally linked resting-state networks reflect the underlying structural connectivity architecture of the human brain. *Hum Brain Mapp 30:3127–3141, 2009.*

Key words: anatomical connectivity; connectivity; DTI; diffusion tensor imaging; fMRI; functional connectivity; resting-state fMRI; resting-state connectivity; white matter

INTRODUCTION

Our brain is never idle. Even when we are at rest, a large number of anatomically separate brain areas show a vast amount of spontaneous neuronal activity and are functionally linked to each other [Biswal et al., 1995; Greicius et al., 2003; Gusnard et al., 2001]. Regions that show such synchronized behavior during rest are said to form *resting-state networks* (RSNs) [Beckmann et al., 2005; Damoiseaux et al., 2006; Greicius et al., 2003; Van den Heuvel et al., 2008a,b]. The high level of functional connectivity between RSN regions suggests the existence of direct anatomical pathways between these brain areas to facilitate

Contract grant sponsor: Dutch Science Organization for Medical Research (VIDI Program); Contract grant numbers: H.E.H.,917.46.370.

*Correspondence to: Martijn van den Heuvel, Rudolf Magnus Institute of Neuroscience, University Medical Center Utrecht, Heidelberglaan 100, 3508 GA Utrecht, PO Box 85500, The Netherlands. E-mail: M.P.vandenheuvel@umcutrecht.nl

Received for publication 28 August 2008; Revised 5 December 2008; Accepted 17 December 2008

DOI: 10.1002/hbm.20737

Published online 23 February 2009 in Wiley InterScience (www.interscience.wiley.com).

this high level of ongoing interregional communication during rest. In this study, we examined the structural connectivity architecture of functionally linked RSNs.

The synchronization of neuronal activity between anatomically separate brain regions is known as functional connectivity [Aertsen et al., 1989; Biswal et al., 1995; Friston et al., 1993; Lowe et al., 2000] and has been investigated by examining the coherence of resting-state functional Magnetic Resonance Imaging time-series [Biswal et al., 1995; Lowe et al., 2000; Xiong et al., 1999]. Of special interest are the low frequency oscillations (0.01–0.1 Hz) of resting-state fMRI BOLD time-series, which show a strong correlation between RSN regions during rest [Biswal et al., 1995; Cordes et al., 2000; Damoiseaux et al., 2006; Lowe et al., 1996; 2000; Xiong et al., 1999]. There is an ongoing debate about whether these coherent patterns predominantly originate from physiological signals, like cardiac or respiratory oscillations [Shmueli et al., 2007; Wise et al., 2004] or whether they truly reflect synchronization of intrinsic neuronal activity. The latter view is supported by the notion that most of these coherent patterns have been found between regions that are known to share a common behavioral or cognitive function [Biswal et al., 1995; Damoiseaux et al., 2006; Xiong et al., 1999]. Furthermore, resting-state BOLD fluctuations have been reported to strongly correlate with concurrent fluctuations in neuronal spiking [Shmuel and Leopold, 2008], linking resting-state fMRI time-series directly to neuronal activation and synchronization [Shmuel and Leopold, 2008]. In addition, a recent study has shown that slow modulations in neuronal spiking are linked to spontaneous fMRI fluctuations in the human sensory cortex (Nir et al., (in press]). In this context, it is believed that the coherence between the resting-state fMRI time-series of anatomically separate cortical regions reflects, at least in part, a high level of functional connectivity between these brain areas.

A number of group studies have reported the consistent formation of RSNs during rest [Beckmann et al., 2005; Damoiseaux et al., 2006; De Luca et al., 2006; Salvador et al., 2005a; Van den Heuvel et al., 2008a,b]. The most commonly found RSNs include the 'default mode network' that links precuneus/posterior cingulate cortex with medial frontal regions and bilateral inferior parietal regions [Damoiseaux et al., 2006; Fox and Raichle, 2007; Greicius et al., 2003; Gusnard et al., 2001], the 'core network' linking bilateral insular regions and anterior cingulate cortex [Dosenbach et al., 2007], two lateralized parietal-frontal networks that are often associated with attentional processing and networks that overlap primary sensorimotor and (extra-striate) visual systems [Beckmann et al., 2005; Biswal et al., 1995; Damoiseaux et al., 2006; Lowe et al., 1998; 2000; Xiong et al., 1999]. Activation of the default mode network and the core network have been suggested to play an important role in core processes of human cognition [Fox and Raichle, 2007; Gusnard et al., 2001], including mind wandering [Mason et al., 2007], goal-directed behavior [Dosenbach et al., 2007] and relating oneself to the outside world [Gusnard et al., 2001].

The high level of functional connectivity within RSNs suggests the existence of direct anatomical connections between these brain areas to support the ongoing information transfer between these regions during rest. White matter pathways are the structural connections of our brain and can be investigated using Diffusion Tensor Imaging (DTI). DTI is a technique to determine the main diffusion direction of water molecules in brain tissue [Basser et al., 2000; Beaulieu and Allen 1994], enabling the reconstruction of the white matter pathways of the brain [Mori and van Zijl, 2002]. Indeed, Greicius et al. [Greicius et al., 2009] demonstrated the existence of direct structural white matter pathways between the regions of the functional default mode network, suggesting an important role for the cingulum tract in connecting the active regions of the default mode network. Indeed, in a recent study we reported a direct association between the microstructural organization of the interconnecting cingulum tract and the level of default mode functional connectivity [Van den Heuvel et al., 2008b]. Furthermore, Lowe et al. [Lowe et al., 2008] recently demonstrated in patients with multiple sclerosis that disease related decreases of functional connectivity between left and right primary motor regions are associated with the structural integrity of interconnecting corpus callosum tracts. In addition, section of the corpus callosum has been reported to result in complete loss of interhemispheric resting-state functional connectivity [Johnston et al., 2008]. These studies support the view that anatomical white matter pathways play an important role in resting-state synchronization. Taken together, they suggest a direct link between structural and functional connectivity in the human brain [Greicius et al., 2009; Hagmann et al., 2007, 2008 #217; Johnston et al., 2008; Koch et al., 2002; Lowe et al., 2008; Van den Heuvel et al., 2008b]. However, it is unknown whether functional RSNs are truly 'hard-wired' in the brain. In other words, are the functionally linked regions of known RSNs directly interconnected by anatomical white matter pathways? If the high level of observed fMRI coherence indeed reflects neuronal synchronization between RSN regions, one would expect an underlying anatomical infrastructure to facilitate the ongoing interregional communication between RSN regions during rest. In this study, we examined the existence of structural white matter bundles between the functionally connected regions of known RSNs as evidence for an anatomical dependence of resting-state networks. We acquired resting-state fMRI BOLD time-series in 26 healthy subjects on a 3 Tesla MR scanner, together with high resolution DTI scans to reconstruct the white matter tracts of the brain. Nine consistently found RSNs were retrieved from the resting-state data. The existence of direct structural connections between the functionally linked RSN regions was examined by combining the RSN maps with DTI based fiber tracking.

MATERIALS AND METHODS

Subjects

Twenty six healthy subjects (age mean: 25, SD: 7.7, 14 male, 12 female) participated in this study after given written consent as approved by the medical ethics committee for research in humans of the University Medical Center, Utrecht, the Netherlands. Resting-state functional Magnetic Resonance Imaging (resting-state fMRI) and Diffusion Tensor Imaging (DTI) data were acquired on a 3 Tesla Philips Achieva Medical Scanner. During the resting-state recordings, the subjects were instructed to relax, keep their eyes closed without falling asleep and to think of nothing in particular. Subjects who reported to have fallen asleep or reported to be close to fallen asleep were excluded and a new subject was included as a replacement, resulting in the described group of 26 subjects.

Image Acquisition

Resting-state Blood Oxygenation Level Dependent (BOLD) signals were recorded during a period of 8 min using a fast fMRI sequence (3D PRESTOSENSE p/s-reduction 2/2, TR/TE = 22/32 ms using shifted echo, slice orientation: sagittal, flip-angle 9 degrees, dynamic scan time 0.5 sec, voxel-size $4 \times 4 \times 4$ mm^3, FOV = $128 \times 256 \times 256$ mm^3, reconstruction matrix = $32 \times 64 \times 64$ covering whole brain). The short volume acquisition time of 500 ms allowed proper sampling of information in the frequency domain up to 1 Hz. This minimized the possible back-folding of possible confounding effects of higher frequencies, such as respiratory and cardiac oscillations ($\sim$0.3 and $>$0.8 Hz, respectively), into the lower frequencies of interest (0.01–0.1 Hz) (Cordes et al., 2001). Functional PRESTO images have a relative low anatomical contrast compared with an anatomical T1 image. Therefore, directly after the functional time-series an additional high contrast PRESTO image was acquired, with identical scanning parameters but with a higher anatomical contrast (i.e., a better contrast between white and grey matter), which was obtained by increasing the flip angle to 25 degrees. This additional high contrast PRESTO image was acquired to improve the coregistration of the resting-state time-series with the T1 image.

In the same scanning session, 2 DTI sets each consisting of 30-weighted diffusion scans and 5 unweighted B = 0 scans (b = 0 s/mm^2) were acquired (DTI-MR using parallel imaging SENSE p-reduction 3; high angular gradientset of 30 different weighted directions (Jones, 2004; Jones et al., 1999), TR/TE = 7035/68 ms, voxel-size $2 \times 2 \times 2$ mm^3, FOV = $240 \times 240 \times 150$ mm^3, reconstruction matrix = $120 \times 120 \times 75$ covering whole brain, b = 0 s/mm^2 for the unweighted scans and b = 1000 s/mm^2 for the weighted scans, second set with reversed k-space read-out). In addition, an anatomical T1 weighted image (3D FFE using parallel imaging; TR/TE = 10/4.6 ms, flip-angle 8 degrees, slice orientation: sagittal, $0.75 \times 0.75 \times 0.8$ mm^3 voxelsize, FOV = $160 \times 240 \times 240$ mm^3, reconstruction matrix = $200 \times 320 \times 320$ covering whole brain) was acquired for anatomical reference.

Image Preprocessing

Preprocessing of the resting-state fMRI data was performed with the SPM2 software package (http://www.fil.ion.ucl.ac.uk). Functional scans were corrected for small head movements by realigning all functional scans to the last scan. Next, the functional time-series and the T1 image were co-registered with the high-contrast functional scan, enabling overlap between the functional resting-state time-series and the T1 image. Cortical voxels were selected based on a cortical segmentation of the T1 image, which was performed with the freely available Freesurfer software package (http://surfer.nmr.mgh.harvard.edu/). The T1 image was spatially normalized (nonlinear) to match the MNI 305 T1 template brain [Collins et al., 1994] and the fMRI time-series and the cortical segmentation map were normalized (nonlinear) to standard space by using the normalization parameters of the T1 image.

To select the low resting-state frequencies of interest (0.01–0.1 Hz) [Biswal et al., 1995; 1997; Cordes et al., 2001], the rest recorded fMRI time-series were bandpass filtered with a finite impulse response (FIR) bandpass filter with zero phase distortion (bandwidth 0.01–0.1 Hz). Filtering eliminated low frequency noise (including slow scanner drifts) and influences of higher frequencies reflecting cardiac and respiratory signals [Cordes et al., 2001].

Preprocessing of the DTI data was performed with the diffusion toolbox of Andersson et al. [Andersson and Skare, 2002; Andersson et al., 2003] and in-house developed software. For each of the 2 DTI sets, the 5 unweighted B = 0 were averaged. In total, this resulted in two averaged unweighted B = 0 images. Next, susceptibility distortions, which are often reported in single-shot EPI images [Andersson et al., 2003], were corrected by combining the two DTI datasets. This correction was performed by computing a field distortion map based on the two averaged unweighted B = 0 images, which were acquired with an opposite k-space read-out direction [Andersson et al., 2003]. The resulting field map was then applied to the two sets of 30 weighted images, resulting in a single set of 30 weighted directions [Andersson et al., 2003]. The DTI images were corrected for small head movements by realigning all weighted scans to the unweighted B = 0 image [Andersson and Skare, 2002]. Within each voxel, the diffusion profile was fitted a tensor using a robust tensor fit method based on M-estimators [Chang et al., 2005]. Next, the main diffusion direction within each voxel was selected as the principal eigenvector, determined by the eigenvalue decomposition of the fitted tensor [Mori et al., 1999; Mori and van Zijl, 2002]. For each individual DTI dataset, the *Fiber Assignment by Continuous Tracking* (FACT) [Mori et al., 1999; Mori and van Zijl, 2002] algorithm was

used to reconstruct the total collection of white matter tracts of the brain, often called *fibers* or *tracts* [Mori et al., 2002]. Twenty seven seeds were started in each voxel. Fiber tracking was stopped when the fiber reached a voxel with a FA value lower than 0.1, when the trajectory of the traced fiber exceeded the brain or when the eigenvector had an average angle of >45 degrees with the main diffusion direction of neighboring voxels.

Selection of Functionally Linked Resting-State Networks

RSNs were retrieved from the resting-state data using the *Normalized Cut Group Clustering* method, as validated earlier [Van den Heuvel et al., 2008a]. In brief, this voxel-based clustering method involved the grouping of voxels that consistently showed a high level of functional connectivity over the group of subjects. The *Normalized Cut Group Clustering* method consists of two clustering stages, being (1) the individual clustering stage and (2) the group clustering stage. First, at Stage 1, from each individual dataset a graph $G = (V,E)$ was formed, with V the collection of points (called nodes or vertices) and E the collection of edges (or connections) between the nodes of the graph. The graph was formed out of all cortical voxels (i.e., the nodes V), selected from the individual cortical segmentation maps. The weights of the connections E between all voxel pairs were computed as the zero-lag temporal correlation between the time-series of the voxels, reflecting their level of voxel-wise functional connectivity. For example, the weight $w(i,j)$ of edge $e(i,j)$ between voxel i and voxel j was computed as the correlation between the resting-state time-series of voxel i and voxel j. Next, the resulting individual connectivity graph G was thresholded, setting all connections to 0 that did not reach the set threshold of 0.4 and all connections to 1 that exceeded the threshold. As such, G was defined as an unweighted unidirectional graph with connections between those voxels that showed a high level of functional connectivity. Next, the resulting individual connectivity graph was clustered, using the *Normalized Cut* graph clustering algorithm [Shi and Malik, 2000]. This resulted in the grouping of functionally linked voxels into resting-state networks. Second, at the group level (Stage 2), the consistency of the individual clustering results was computed to determine which voxels consistently showed a high level of functional connectivity over the group of subjects. First, the consistency of the individual clustering results was represented as a *group graph.* The connections between the voxels in the group graph (i.e., the voxels of the group averaged anatomical image) were defined as the level of *cluster-consistency* over the group of subjects. This was performed by defining $w(i,j)$ of edge $e(i,j)$ between voxel i and j in the *group graph* as the total number of times voxel i and j were clustered into the same cluster over the group of subjects. As such, a high weight $w(i,j)$ expressed that in a high number of subjects voxel i and j showed a high level of functional connectivity and were therefore clustered into the same RSN, indicating that over the group of subjects these voxels were likely to belong to the same RSN. As a result, the weights of the *group graph* expressed which voxels consistently showed a high level of functional connectivity over the group of subjects. Second, the resulting group graph was clustered, clustering the voxels into group RSNs that consistently showed a high level of functional connectivity over the group of subjects and grouping voxels into different RSNs that showed a low level of functional connectivity over the group of subjects. Using the *Normalized Cut Group Clustering* procedure, the optimal number of group clusters (i.e., the number of group RSNs) was determined as an optimal clustering fit of the *group graph*, based on minimizing the total *normalized cut cost* to partition the graph into separate networks. As a result, the number of group RSNs was determined automatically, avoiding manual selection of RSNs [Van den Heuvel et al., 2008a].

Group clustering revealed nine RSNs (shown in Fig. 2a), including the default mode network (Fig. 2a, RSN a, red regions), two lateralized parietal-frontal networks consisting of superior parietal and superior frontal regions (Fig. 2a, RSN b and c, green and blue regions), a network consisting of primary motor regions (Fig. 2a, RSN d, dark green regions), a network consisting of primary visual regions (Fig. 2a, RSNd, dark blue regions), a network consisting of extra-striate visual regions (Fig. 2a, RSNd, orange regions), a network overlapping bilateral insular regions and anterior cingulate cortex (ACC) (Fig. 2a, RSN e, pink regions) and two singular networks consisting of bilateral medial frontal cortex (Fig. 2a, RSN f, light blue regions) and posterior precuneus regions (Fig. 2a, RSN g, light brown regions). Please see the results section and Table I for a full description of the RSN regions.

Structural Connections Between Functionally Linked RSN Regions

To examine the existence of structural connections between the functionally linked RSN regions the DTI fiber data was combined with the nine RSN clustermaps. The selection of interconnecting anatomical tracts between RSN regions was performed in a 3-step procedure, illustrated in Figure 1. First, for each individual dataset, the total collection of reconstructed fibers was selected (Fig. 1a). Second, from each of the nine RSNs, a first region of interest (ROI) was appointed and from the total collection of reconstructed fibers the tracts that reached this first ROI were selected (Fig. 1b). To improve the penetration of the reconstructed tracts into the RSN regions of interest, the ROIs were dilated with a maximum of 4 mm (i.e., 1 fMRI voxel). Third, a second ROI was selected from the RSN clustermap (Fig. 1**c**) and from the resulting fibers of the previous step, only the tracts that also reached the second ROI were selected. This procedure resulted in the tracts that connected both ROIs (Fig. 1c). Next, as this procedure was completed for all subjects, the individual interconnecting

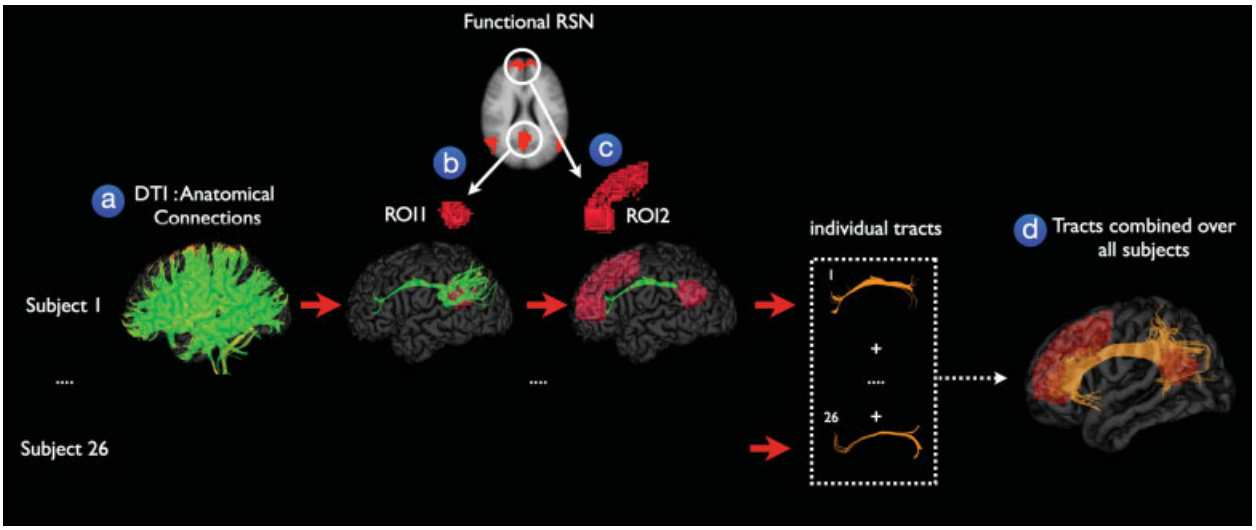

Figure 1.

Structural connections between functionally connected resting-state network regions. The existence of possible anatomical white matter tracts between functionally connected resting-state network (RSN) regions was examined in a 3-step procedure. First, for each individual, the DTI data was used to reconstruct the white matter tracts of the human brain, called *fibers* or *tracts* (step a). Second, for each of the nine functionally connected RSNs, a first region of interest (ROI) was selected and from the total collection of fibers, the tracts that reached the first ROI were selected (step b). Third, a second ROI was retrieved from the RSN clustermap and from the resulting tracts of the previous step, only the tracts that reached this second ROI were selected (step c). For illustration purposes, the individual interconnecting tracts were normalized to match standard space (MNI 305) and combined over the group of subjects. The combined tracts represented the existence of a direct anatomical white matter connection between the functionally connected regions of a known resting-state network.

tracts were normalized to match standard space (MNI 305) using the normalization parameters of the B = 0 image and combined over the group of subjects. Individual tracts were combined by bundling the individual tracts over the group of subjects, such that the total collection of tracts reflected all the tracts between ROIa and ROIb of subject 1–subject 26 (Fig. 1d).

Group Consistency Maps

To examine the consistency of the interconnecting white matter pathways between RSN regions over the group of subjects, for each interconnecting tract within each RSN a *group consistency flag map* was computed. This group consistency flag map served as an indicator of which white matter regions were consistently crossed over the group of subjects by the interconnecting fiber tracts. This was performed in a 3-step procedure. First, for each individual dataset, the interconnecting fibers between the two selected RSN regions were selected and an individual 3D volume was created, flagging those voxels that were crossed by the interconnecting fibers. Voxels that were crossed by 1 or more fibers were flagged with a value of 1, resulting in an individual binary flag map. Second, in the group stage, the individual flag maps were summated providing a *group consistency flag map*, indicating the overlap of the found interconnecting tracts over the group of subjects. As such, white matter regions that were consistently crossed by the interconnecting fibers over the group of subjects were indicated with a high voxel value. This procedure was repeated for all RSNs.

RESULTS

Resting-State Networks

Normalized Cut Group Clustering of the resting-state fMRI time-series of the 26 subjects revealed 9 RSN, as validated earlier [Van den Heuvel et al., 2008c]. These functionally linked networks included the *default mode network*, the *core network*, two lateralized parietal-frontal networks, primary motor, primary visual, extra-striate visual network and two singular networks consisting of bilateral medial frontal regions and posterior parietal cortical regions. The nine RSNs are shown in Figure 2 (panel a). RSN a (Fig. 2a, RSN a) shows the default mode network [Greicius et al., 2003; Gusnard et al., 2001; Raichle et al., 2001; Raichle and Snyder, 2007] overlapping posterior cingulate/precuneus region (Brodmann Area (BA) 23/31), inferior and superior parietal cortex (BA 39/40), superior frontal gyrus (BA 8) and medial frontal gyrus (BA 8/9/10/11) [Damoiseaux et al., 2006]. RSN b and c (Fig. 2a, RSN b and c) reflect lateralized parietal-frontal networks in the left and right

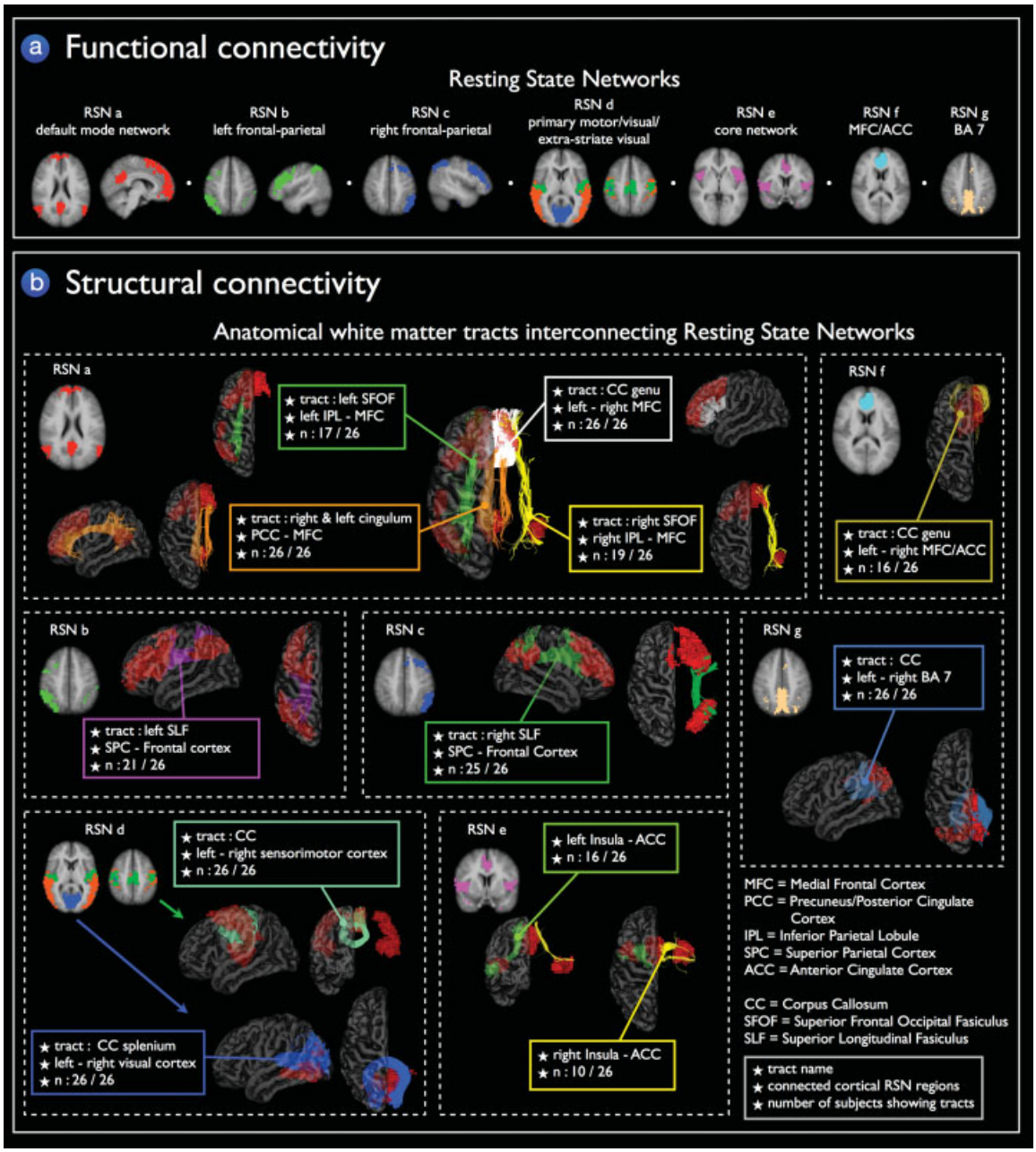

Figure 2.

Structural connections of the functionally linked resting-state networks. Group clustering of the resting-state fMRI data revealed nine resting-state networks (RSNs) of functionally linked cortical regions (panel **a**). Fiber tracking DTI data revealed interconnecting white matter pathways in eight of these nine RSNs in a substantial proportion of the group of subjects (panel **b**). Panel a Functional connectivity: Resting-State Networks. The nine networks included the default mode network (RSN a, red network), two lateralized parietal-frontal networks (RSN b green network and RSN c blue network), primary motor, visual, and extra-striate visual networks (RSN d, green, blue and orange networks, respectively), the core network consisting of bilateral insular regions and regions overlapping the anterior cingulate cortex (RSN e pink network) and two networks consisting of bilateral regions overlapping medial frontal cortex/anterior cingulate cortex (RSN f light blue network) and regions overlapping left and right posterior precuneus (BA 7) (RSN g light brown network). Panel b, Structural connectivity: Anatomical white matter tracts interconnecting resting-state networks. Fiber tracking DTI data revealed interconnecting white matter pathways in eight of the nine RSNs in a substantial proportion of the group of subjects. The *cingulum* tract, bilateral *superior frontal occipital fasciculus* (*SFOF*), and the *genu of the corpus callosum* (*CC*) were found to interconnect the regions of the default mode network (RSN a orange, green/yellow and white tracts). The functionally linked regions of the lateralized parietal-frontal networks were found to be interconnected by the *superior longitudinal fasciculus* (*SLF*) (RSN b purple tracts, RSN c green tracts). *Corpus callosum* (*CC*) tracts interconnected the regions of the motor network (RSN d mint green fibers) and the regions of the visual network (RSN d blue tracts). Left and right insular regions and anterior cingulate cortex of the core network were found to be interconnected by white matter tracts (RSN e, green and yellow tracts, respectively) in part of the group of subjects. Finally, the bilateral regions of the two singular networks RSN f and RSN g were found to be interconnected by *corpus callosum* tracts (RSN f dark yellow tracts and RSN g grey blue tracts). *Fiber information boxes* provide information about the name of the interconnecting tract, the functionally linked cortical regions and the number of *N* subjects of the group of 26 subjects that showed these interconnecting tracts (N/26).

hemisphere, including cortical regions of the superior parietal lobule, supramarginal gyrus (BA 7/40) and the middle and superior frontal gyrus (BA 8/9). RSN d (Fig. 2a, RSN d) consisted of postcentral gyrus (BA 3/1/2), precentral gyrus (BA 4), cingulate gyrus (BA 24) and lateral, medial and superior occipital gyrus and peristriate regions (BA 17/18/19). The motor and visual regions of RSNd were originally clustered as a single RSN [Van den Heuvel et al., 2008c], suggesting a high level of functional connectivity between primary motor and primary (extra-striate) visual regions. Most other studies have reported the motor and visual networks as two separate RSNs, although a recent study has provided supporting evidence for a high level of functional connectivity between motor and visual regions by also reporting these regions as a single RSN [Vincent et al., 2008]. To examine the existence of sub-networks within this combined motor/visual network, a second level clustering was performed on the voxels in the combined motor/visual RSN (RSNd) [Van den Heuvel et al., 2008a]. As expected, this resulted in the clustering of separate sub-networks for the primary motor, primary visual and extra-striate visual regions. These sub-networks are shown in RSN d of Figure 2a, including a separate primary sensorimotor network (Fig. 2a, RSN d, green cluster), a visual network (Fig. 2a, RSN d, blue cluster) and a network consisting of bilateral extra-striate visual regions (Fig. 2a, RSNd, orange cluster) [Biswal et al., 1995; Damoiseaux et al., 2006; Salvador et al., 2005a; Xiong et al., 1999]. Furthermore, RSN e (Fig. 2a, RSN e) shows the so-called *core network* [Dosenbach et al., 2007] consisting of bilateral insular and superior temporal cortex (BA 21/22) and a part of the cingulate gyrus (BA 24). RSN f (Fig. 2a, RSN f) overlaps bilateral regions of the medial frontal gyrus (BA 9) and an anterior part of the cingulate gyrus (BA 32) [Damoiseaux et al., 2006]. Finally, RSN g (Fig. 2a, RSN g) consisted of a singular region overlapping a posterior part of bilateral precuneus (BA 7).

Anatomical White Matter Tracts Interconnecting Resting-State Networks

Well-known anatomical white matter tracts [Schmahmann and Pandya, 2006; Schmahmann et al., 2007; Vogt and Pandya, 1987; Wakana et al., 2004] were found to interconnect eight of the nine functionally linked RSNs across the group of subjects. Figure 2a,b shows a general overview of all RSNs and the white matter tracts that were found to interconnect the RSN regions. Figures 3–7 show the RSNs and the interconnecting tracts in more detail, together with the matching *group consistency flag maps*. In addition, Table I describes the functionally linked regions of the nine RSNs (RSN a to g) and the interconnecting white matter tracts that were found to interconnect the RSN regions.

RSN a

Figure 3 shows the interconnecting tracts of the regions of the so-called *default mode network* [Greicius et al., 2003; Gusnard et al., 2001; Raichle et al., 2001; Raichle and Snyder, 2007]. The *cingulum* tract (Fig. 3, RSN a orange tracts, 26 of 26 subjects showed interconnecting fibers (26/26)) [Greicius et al., 2009], the left and right *superior frontal-occipital fasciculus* (green and yellow tracts, 17/26 and 19/26) and the *genu* of the *corpus callosum* (white tracts, 26/26) were found to interconnect the active areas within the default mode network. The matching *group consistency flag maps* suggest a high level of consistency of the interconnecting tracts over the group of subjects. The consistency flag maps show high voxel values for the center line of the *cingulum,* i.e., group consistency voxel values of over 15 were found, indicating that the trajectories of the interconnecting tracts of more than 15 subjects of the group of 26 all crossed overlapping voxels. Similarly, the group consistency maps for the *genu* tract showed high consistency voxel values (i.e., >12), also indicating a high level of consistency over the group of subjects. Please note that no spatial smoothing was applied to the group consistency flag maps.

RSN b and c

The two lateralized parietal-frontal RSNs were found to be interconnected by the left and right structural *superior longitudinal fasciculus* [Wakana et al., 2004] (Fig. 4, RSN b purple tracts, 21/26 and RSN c dark green tracts, 25/26). The group consistency flag maps of these interconnecting tracts are shown in Figure 4, suggesting a high level of consistency of the interconnecting tracts over the group of subjects (showing group consistency voxel values of over 15 in both left and right hemispheric tracts).

RSN d

Tracts of the *body* of the *corpus callosum* were found to interconnect the primary sensorimotor network (Fig. 5, RSN d mint green tracts, 26/26) and tracts crossing the *splenium* of the *corpus callosum* were found to interconnect the regions of the primary visual network (RSN d blue tracts, 26/26). Similar to the other RSNs these interconnecting tracts were found with a high level of consistency over the group of subjects, indicated by group consistency voxel values of over 15 (see Fig. 5). No interconnecting tracts were found between the extra-striate visual regions (Fig. 2a, RSNd, orange network).

RSN e

In part of the group of subjects (16 of 26 and 10 of the group of 26 subjects, respectively) white matter tracts were found to interconnect the regions of the *core network* (Fig. 6, RSN e, green and yellow tracts) [Vogt and Pandya, 1987]. Figure 6 shows the interconnecting tracts between the left and right insular regions and the anterior cingulate cortex and the matching group consistency flag maps of

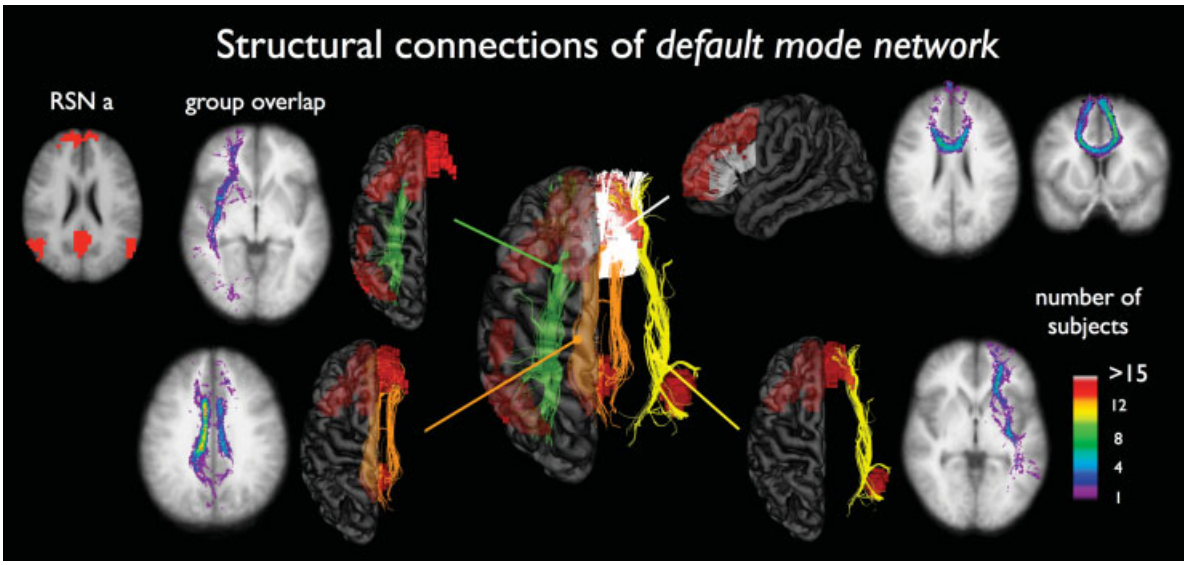

Figure 3.

Structural white matter tracts between regions of the default mode network (RSN a). Figure shows that the cingulum tract (orange tracts, 26 of 26 subjects showing interconnecting tracts), the left and right superior frontal-occipital fasciculus (green 17/26 and yellow tracts 19/26), and the genu of the corpus callosum (26/26 subjects) play an important role in interconnecting the regions of the default mode network. The matching group consistency flag maps show large overlap over the group of subjects, especially for the cingulum (maximum consistency voxel values of 15) and genu tracts (voxel values of 12). The group consistency flag maps indicate for each voxel how many subjects of the group of 26 subjects showed interconnecting tracts between the two RSN regions that touched this particular white matter region. Please note that no spatial smoothing was applied to the group consistency flagmaps.

the found tracts (group consistency values of 5 and 3, respectively).

RSN f and g

Fibers passing the *genu* of the *corpus callosum* were found to interconnect the left and right prefrontal cortical regions of RSN f, shown in Figure 6 (RSN f, dark yellow tracts) in 16 of the 26 subjects (maximum group consistency values of 15). Finally, interhemispheric *corpus callosum* tracts were found to interconnect the left and right posterior precuneus regions of RSN g (Fig. 6, RSN g grey blue tracts, 26 of 26 subjects showing tracts, maximum group consistency values of 12).

DISCUSSION

Multiple brain regions are functionally linked to each other during rest, forming *resting-state networks* (RSNs) [Biswal et al., 1995; Fox and Raichle, 2007; Greicius et al., 2003]. This study demonstrates that almost all of these functionally linked RSNs are interconnected by anatomical white matter tracts [Wakana et al., 2004]. Our findings strongly suggest that functionally linked resting-state networks have an underlying structural core.

The nine examined RSNs are commonly found in resting-state group studies [Beckmann et al., 2005; Damoiseaux et al., 2006; De Luca et al., 2006; Salvador et al., 2005a] (Fig. 2a). In particular, eight of the nine group clustered RSNs show one-on-one overlap with the group ICA components reported by Damoiseaux et al. [Damoiseaux et al., 2006], including the *default mode network* (RSN a), the lateralized parietal-frontal networks (RSN b and c), the primary motor, visual and extra-striate visual sub-networks (RSN d), the *core network* consisting of bilateral insular and ACC regions (RSN e) and the network overlapping bilateral posterior medial frontal regions (RSN f). Only the network consisting of posterior precuneus regions (RSN g) was not reported by Damoiseaux et al. The high overlap between the found RSNs of our study and the networks found by Damoiseaux et al. provide strong evidence for the robust formation of functional RSNs in the human brain during rest.

The focus of our study was on the identification of white matter tracts between functionally linked RSN regions. Well-known white matter tracts [Wakana et al., 2004] were found to interconnect the functionally linked regions in eight of nine commonly found RSNs. Specifically, we found an important role for the tracts of the *cingulum, superior frontal-occipital fasciculus* and *genu of the*

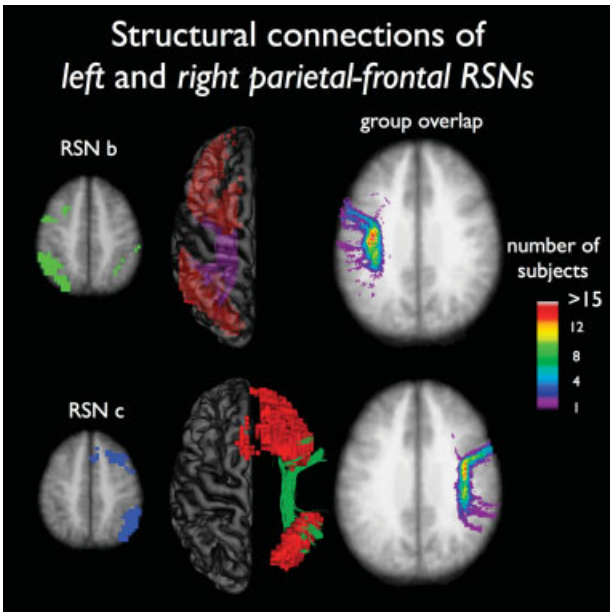

Figure 4.

Structural white matter connections between regions of the two lateralized parietal-frontal networks (RSN b and c). Figure shows an important role for the left and right superior parietal fasciculus to interconnect the functionally linked middle/superior frontal and superior parietal regions in the left (21 of 26 subjects showed interconnecting tracts) and right hemisphere (25 of 26 subjects showed interconnecting tracts). The group consistency maps show large overlap over the group of subjects (maximum group consistency voxel values of over 15).

corpus callosum [Wakana et al., 2004] in interconnecting the active regions of the default mode network (see Fig. 3). The *group consistency flag maps*, reflecting the overlap of the found interconnecting tracts over the group of subjects suggest a high level of consistency of these tracts over the group of subjects, especially for the cingulum and genu tracts (see Fig. 3). These results are supported by recent findings, demonstrating an important interconnecting role for the cingulum tract in the default mode network [Greicius et al., 2009; Heuvel et al., 2008b]. Furthermore, the left and right *superior longitudinal fasciculus* [Wakana et al., 2004] were found to interconnect the two lateralized parietal-frontal RSNs (see Fig. 4). In addition, distinct interhemispheric *corpus callosal* tracts [Wakana et al., 2004] were found to interconnect the regions of the primary motor network [Lowe et al., 2008] and the regions of the visual network with a high level of consistency over the group of subjects (see Fig. 5). Furthermore, corpus callosum tracts were found to interconnect the regions of the two singular resting-state networks, overlapping bilateral prefrontal and posterior precuneus regions (see Fig. 7).

Five of the nine clustered group RSNs consist of homologous regions, being the primary motor, primary visual, extra-striate visual and the RSNs consisting of bilateral prefrontal (RSN f) and posterior precuneus regions (RSN g). Given that most homologous regions are interconnected by corpus callosal tracts, the existence of direct structural connections between these RSN regions was expected. However, the other four RSNs, including the default mode network, core network and the two parietal-frontal networks do not (only) consist of homologous regions, but rather consist of lateralized brain regions. Therefore, the existence of interconnecting white matter tracts between these functionally linked RSN regions strongly supports the notion of a structural core of RSNs in the human brain.

White matter pathways are bundles of huge numbers of axons that connect large neuronal populations over long distances [Schmahmann and Pandya, 2006; Schmahmann et al., 2007; Vogt and Pandya, 1987; Wakana et al., 2004]. They are the structural highways of our brain, enabling information to travel quickly from one region to another.

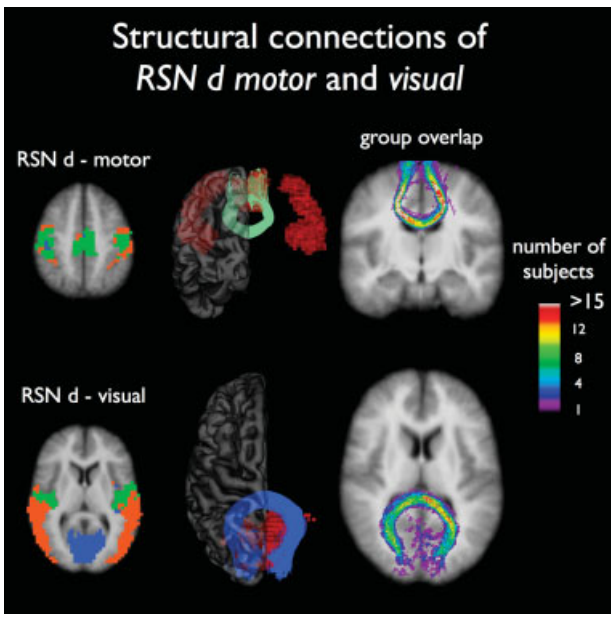

Figure 5.

Interconnecting tracts between regions of the primary motor and primary visual resting-state network (RSNd). Figure shows an important role for corpus callosum tracts to interconnect the regions of the primary motor (green RSN, 26 of 26 subjects showing tracts) and primary visual resting-state network (blue RSN, all 26 subjects showing tracts). No interconnecting tracts were found between the homologous regions of the extra-striate visual network (orange RSN), which is likely to result from the difficulty of tracing fibers that cross other large fiber bundles. The group consistency flag maps show a large consistency of the found interconnecting tracts over the group of 26 subjects (maximum consistency values of over 15).

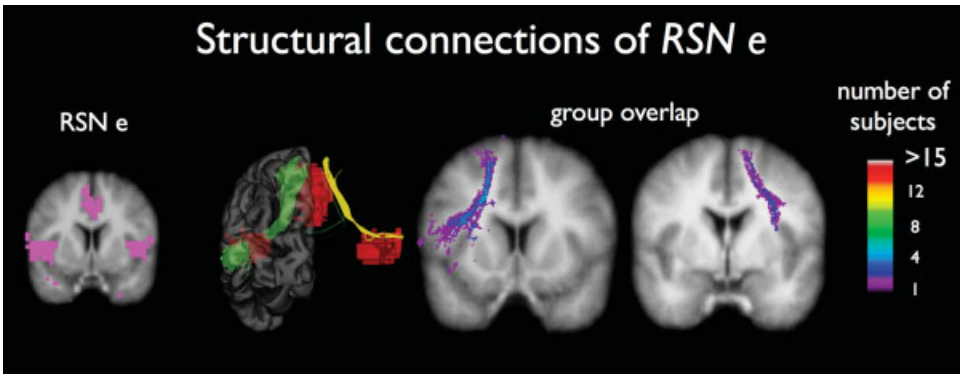

Figure 6.

Interconnecting tracts between regions of the core network (RSN e). Fiber tracking revealed interconnecting tracts between the ACC region and the left/right insular regions of RSN e in part of the subjects (16 of 26 and 10 of 26, respectively). Group consistency maps showed a high variation of the interconnecting tracts over the group of subjects, indicated by the maximum consistency voxel values of 5 and 3, respectively.

The notion that functionally linked RSN regions are directly interconnected by these structural highways suggests that RSN activity and synchronization indeed reflect ongoing information integration between anatomically separate regions during rest [Greicius et al., 2003; 2009]. This supports the view that RSNs are meaningful networks [Dosenbach et al., 2007; Fox and Raichle, 2007; Greicius et al., 2003; Gusnard et al., 2001; Mason et al., 2007]. Our results do not directly provide information about the functional relevance of RSNs, but other studies have indicated that activity of at least the default mode network and the core network may play an important role in human cognition. Regions of the core network have been associated with the processing of salient stimuli [Seeley et al., 2007] and goal-directed behavior [Dosenbach et al., 2007] and activation of the default mode network has been linked to mind-wandering [Mason et al., 2007], relating oneself to the outside world [Gusnard et al., 2001] and integration of cognitive and emotional processing [Greicius et al., 2003]. These cognitive processes are likely to continue during rest [Greicius et al., 2003; Gusnard et al., 2001] and anatomical white matter pathways between these functionally linked RSN regions could facilitate this ongoing information integration between these regions.

Functional connections between multiple cortical brain regions were examined by computing the correlation between fMRI time-series measured during rest [Achard et al., 2006; Salvador et al., 2005b; Van den Heuvel et al., 2008b]. However, when correlation is used as a measure of functional connectivity, it is unclear whether a high level of functional connectivity between two regions is reflecting *direct* communication between these regions, or whether these regions are *indirectly* linked through a third party region. As DTI only measures the *direct* structural connections between brain regions and resting-state fMRI may express both *direct* and *indirect* connections the functional and structural connectivity results may only partially overlap. The results of our study demonstrate that a large number of functionally linked RSN regions are directly

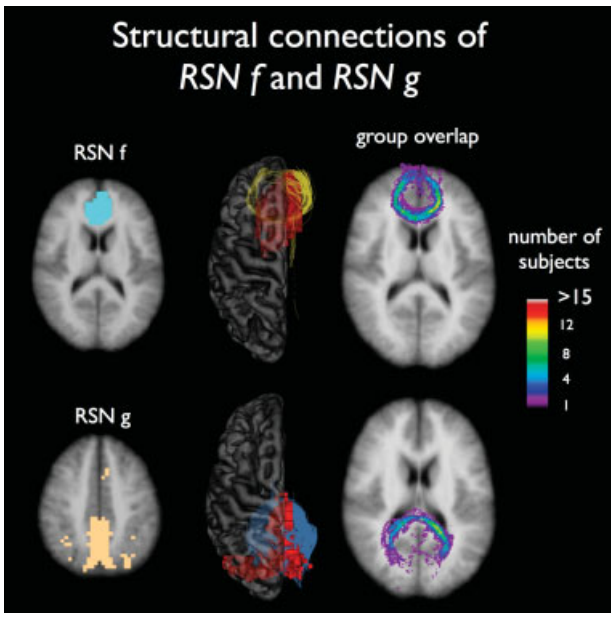

Figure 7.

Interconnecting tracts between homogeneous brain regions of RSN f and RSN g. Corpus callosum tracts were found to interconnect the bilateral medial frontal regions of RSN f (16 of 26 subjects showed tracts) and the bilateral posterior precuneus regions of RSN g (all 26 subjects showed interconnecting tracts), with a high level of consistency over the group of subjects (maximum consistency values of 15 and 12, respectively).

TABLE I. Functional and structural connections of resting state networks

Resting state network	*Name*	*Functionally linked regions*	*Structural connections*
RSN a	default mode network	MFC (left, right)	genu of corpus callosum; cingulum; left superior fronto-occipital fasciculus; right superior fronto-occipital fasciculus
		PCC	
		left IPL	
		right IPL	
RSN b	left parietal-frontal	left SPC	left superior parietal fasciculus
		left SFC	
RSN c	right parietal-frontal	right SPC	right superior parietal fasciculus
		right SFC	
RSN d	primary motor	left motor	body of corpus callosum
		right motor	
	primary visual	left visual	splenium of corpus callosum
		right visual	
	extra-striate visual	left extra-striate	
		right extra-striate	
RSN e	core network	left insular cortex	
		right insular cortex	
		ACC	
RSN f	poserior medial frontal network	left MFC	genu of corpus callosum
		right MFC	
RSN g	posterior precuneus network	left posterior prec	corpus callosum
		right posterior prec	

Table describes the functionally linked regions of the nine clustered RSNs (a – g) and the, interconnecting structural white matter pathways shown in Figure 2b and Figure 3 – 7. MFC, medial frontal cortex; PCC, precuneus/posterior cingulate cortex; IPL, inferior parietal lobule; SFC, superior frontal cortex; SPC, superior parietal cortex; ACC, anterior cingulate cortex; prec, precuneus. [Color table can be viewed in the online issue, which is available at www.interscience.wiley.com.]

structurally interconnected. This suggests that a large number of the functional connections between RSN regions are likely to reflect *direct* connections, as at least the structural infrastructure is present to support direct functional synchronization between these regions. *Partial correlation* has been successfully used to measure the unique level of functional connectivity between two brain regions, by factoring out the influence of third-party regions, expressing only the direct functional connections between two regions [Achard et al., 2006; Liu et al., 2008; Salvador et al., 2005b; Van den Heuvel et al., 2008b]. Future studies of our lab are aimed to specifically examine the *direct* functional and structural connections between RSN regions [Van den Heuvel et al., 2008b].

Supporting evidence for a structural core of functional RSNs comes from studies who report on decreased functional connectivity in combination with studies how report on degenerative effects of the microstructural organization of white matter tracts. Aging has been related to reduced resting-state activity [Damoiseaux et al., 2008] and decreased levels of fractional anisotropy of white matter [Makris et al., 2007; Schneiderman et al., 2007; Yoon et al., 2007]. Reduced activity of the default mode network has been directly related to an altered microstructural organization of the cingulum tract in advanced aging and decreased levels of cognitive performance [Andrews-Hanna et al., 2007]. In addition, disease related decreases of functional connectivity in patients with multiple sclerosis have been associated with decreased structural integrity of corpus callosum fibers [Lowe et al., 2008]. Furthermore, patients with psychiatric diseases, such as schizophrenia, that are known to have (progressive) structural gray matter change [Hulshoff Pol and Kahn, 2008; Hulshoff Pol et al., 2001] have been reported to show both altered resting-state activity [Bluhm et al., 2007; Liang et al., 2006; Liu et al., 2006; 2008; Salvador et al., 2007] and altered organization of white matter [Hulshoff Pol et al., 2004; Kubicki et al., 2005; 2007; Nestor et al., 2007; Sun et al., 2003].

Our findings suggest that functionally linked RSNs have an underlying structural connectivity core. The functionally linked RSNs are represented as separate networks that consist of distinct brain regions showing a high level of coherence between their resting-state fMRI time-series. Almost all of the commonly reported RSNs were found to be directly interconnected by known white matter tracts. In this context, it is reasonable to speculate about the idea that direct structural connections between two anatomically separate brain regions may be a precondition for large brain regions to be (direct) functionally linked. As such, our findings support the notion that white matter pathways may be crucial to support the ongoing neuronal communication between anatomically separated brain regions during rest [Greicius et al., 2009; Hagmann et al., 2008; Van den Heuvel et al., 2008b]. However, this does not imply that all structural connected regions should show a high level of functional connectivity during rest. Furthermore, our study suggest the existence of white matter connections between large brain regions of widespread networks. This does not implicate that local functional connectivity is exclusively related to the existence of structural connections between these regions [Koch et al., 2002].

Nine RSNs were found in our study. However, we by no means try to suggest that our functional brain consists of independent functional networks. Rather, we strongly believe that our brain is an integrated dynamic network [Achard and Bullmore, 2007; Hagmann et al., 2007; 2008; Van den Heuvel et al., 2008c], with a vast amount of interaction between multiple RSNs and the existence of both functional and structural connections between RSNs [Hagmann et al., 2007; 2008; Sridharan et al., 2008; Vincent et al., 2008]. Our study adds to the accumulating evidence that our brain is an integrated network of interconnected regions [Achard and Bullmore, 2007; Hagmann et al., 2008; Liu et al., 2008; Stam, 2004; Van den Heuvel et al., 2008c]. Recent studies have shown that the brain network has a so-called *small-world* architecture [Achard and Bullmore, 2007; Hagmann et al., 2008; Micheloyannis et al., 2006; Stam, 2004; Stam et al., 2007; Van den Heuvel et al., 2008c], meaning that its functional and structural connections are organized in an highly efficient manner [Achard and Bullmore, 2007; Hagmann et al., 2007; 2008]. Small-world networks are known to have a high level of both local and global efficiency [Latora and Marchiori, 2001; Achard and Bullmore, 2007], suggesting that information can be efficiently processed locally and then quickly transported to remote regions for further processing. Our results suggest that the cortico-cortical white matter pathways of our brain play an important role in the efficient integration of information within functionally linked RSNs during rest.

We used deterministic fiber tracking [Mori et al., 1999; Mori and van Zijl, 2002] to examine the existence of white matter pathways between functionally linked RSN regions. An alternative approach would be the use of probabilistic fiber tracking. Probabilistic fiber tracking, as for example implemented in the FSL software package, measures the probability that a seed region is connected to a second region. Probabilistic fiber tracking has the advantage that individual connectivity probability maps can be compared between subjects, enabling a statistical group analysis. However, probabilistic fiber tracking does not directly measure the true structural connections between brain regions, but rather the probability that two regions are connected [Jones, 2008]. As the focus of our study was on the identification of the structural white matter pathways between RSN regions, deterministic fiber tracking was used.

Some limitations have to be considered when interpreting the results of this study. First, not all subjects showed interconnecting tracts between all RSN regions. A limited number of subjects showed interconnecting tracts between the regions of the core network (i.e., 10 and 16 of the 26 subjects showed interconnecting tracts) and between the bilateral regions of RSN f (Fig. 2b, RSN f, brown tracts, 10/16). In addition, no interconnecting tracts were found between the two bilateral insular regions of the core network (Fig. 2a, RSN e) and between the regions of the extra-striate visual network (Fig. 2a, RSN d orange regions). The inability to track fibers between these regions could be related to the difficulty of reconstructing tracts that cross other white matter bundles [Wakana et al., 2004]. This is coherent with other studies who report on the difficulty of reconstructing interhemispheric callosal white matter tracts [Basser et al., 2000; Wakana et al., 2004]. Furthermore, fiber tracking only revealed white matter tracts between parts of the RSN regions. The interconnecting tracts shown in Figures 1, 2b and Figures 3–7 suggest that only sub-parts of the ROIs are structurally interconnected. This might indicate that functionally linked RSNs are structurally interconnected in a somewhat hier-

archical fashion, meaning that only sub-parts of a RSN region are directly structurally connected to the other regions of the network and that the other sub-parts of the ROI are in turn connected to these structural connectivity hubs. However, our findings do not provide direct evidence for this. The inability of finding fibers between all parts of two functionally linked ROIs could also be related to the limitations of the used fiber tracking method. Large fiber bundles disperse just before they enter the cortex, which could affect the directionality measurement in the white matter (i.e., lower FA) and hence affect the fiber tracking. Second, individual interconnecting tracts between the functionally linked RSN regions were selected based on group ROIs, which were selected from a group clustering of the resting-state data (Fig. 2a). An alternative approach would be the use of individual ROIs instead of group ROIs to better account for individual anatomical differences of the human brain. However, little is known about individual differences in RSN formation. Up till now most resting-state studies have focused on the identification of RSNs across subjects [Beckmann et al., 2005; Damoiseaux et al., 2006]. As the focus of our study was on the identification of possible interconnecting structural tracts between regions of known RSNs, group ROIs were used to minimize the possible effects of unknown individual differences in RSN formation. However, it is of high interest to examine whether individual differences in functional connectivity between RSN regions is related to individual variation of the interconnecting white matter pathways of the human brain. Third, in this study we focused on cortical regions of RSNs and the existence of cortico-cortical structural connections between these regions. However, sub-cortical regions have also been reported to be involved in RSNs [Beckmann et al., 2005; Damoiseaux et al., 2006; Greicius et al., 2003]. For example, intrinsic functional connections between the thalamus and cortical regions have been reported to be highly region specific [Zhang et al., 2008] and tend to show strong overlap with the structural projections of the thalamus [Behrens et al., 2003]. Fourth, our study shows the existence of interconnecting structural pathways between a large number of functionally linked RSN regions. However, in theory, our data could also be explained by the fact that the fiber tracking reveals structural connections between any two arbitrary brain regions. However, given the special small-world organization of the structural connections of the brain [Hagmann et al., 2007; 2008] we believe that this alternative explanation is highly unlikely. A small-world organization indicates that not every brain region is connected to every other region in the brain, but rather that the number of white matter pathways is limited [Watts and Strogatz, 1998] [Hagmann et al., 2008]. There has to be noted that we do not suggest that our brain consists of fully independent functionally and structurally connected networks. Rather, our brain is likely to be a fully integrated network [Achard et al., 2006; Hagmann et al., 2008; Van den Heuvel et al., 2008c], indicating the existence of both functional and structural connections *between* RSN networks. Future studies are needed to examine these inter-RSN connections.

The main finding from this study is the existence of structural white matter connections between the functionally linked regions of resting-state networks. Twenty six healthy subjects were scanned with 3 Tesla resting-state fMRI recordings and DTI scans to examine both the functional and structural connections of the human brain. Almost all of the commonly reported functional resting-state networks were found to be interconnected by known structural white matter tracts. Our results suggest that functionally linked resting-state networks reflect the underlying structural connectivity architecture of the human brain.

REFERENCES

Achard S, Bullmore E (2007): Efficiency and cost of economical brain functional networks. PLoS Comput Biol 3:e17.

Achard S, Salvador R, Whitcher B, Suckling J, Bullmore E (2006): A resilient, low-frequency, small-world human brain functional network with highly connected association cortical hubs. J Neurosci 26:63–72.

Aertsen AM, Gerstein GL, Habib MK, Palm G (1989): Dynamics of neuronal firing correlation: Modulation of "effective connectivity". J Neurophysiol 61:900–917.

Andersson JL, Skare S (2002): A model-based method for retrospective correction of geometric distortions in diffusion-weighted EPI. Neuroimage 16:177–199.

Andersson JL, Skare S, Ashburner J (2003): How to correct susceptibility distortions in spin-echo echo-planar images: Application to diffusion tensor imaging. Neuroimage 20:870–888.

Andrews-Hanna JR, Snyder AZ, Vincent JL, Lustig C, Head D, Raichle ME, Buckner RL (2007): Disruption of large-scale brain systems in advanced aging. Neuron 56:924–935.

Basser PJ, Pajevic S, Pierpaoli C, Duda J, Aldroubi A (2000): In vivo fiber tractography using DT-MRI data. Magn Reson Med 44:625–632.

Beaulieu C, Allen PS (1994): Water diffusion in the giant axon of the squid: Implications for diffusion-weighted MRI of the nervous system. Magn Reson Med 32:579–583.

Beckmann CF, DeLuca M, Devlin JT, Smith SM (2005): Investigations into resting-state connectivity using independent component analysis. Philos Trans R Soc Lond B Biol Sci 360:1001–1013.

Behrens TE, Johansen-Berg H, Woolrich MW, Smith SM, Wheeler-Kingshott CA, Boulby PA, Barker GJ, Sillery EL, Sheehan K, Ciccarelli O Thompson AJ, Brady JM, Matthews PM (2003): Non-invasive mapping of connections between human thalamus and cortex using diffusion imaging. Nat Neurosci 6:750–757.

Biswal B, Yetkin FZ, Haughton VM, Hyde JS (1995): Functional connectivity in the motor cortex of resting human brain using echo-planar MRI. Magn Reson Med 34:537–541.

Biswal BB, Van Kylen J, Hyde JS (1997): Simultaneous assessment of flow and BOLD signals in resting-state functional connectivity maps. NMR Biomed 10:165–170.

Bluhm RL, Miller J, Lanius RA, Osuch EA, Boksman K, Neufeld R, Theberge J, Schaefer B, Williamson P (2007): Spontaneous low-frequency fluctuations in the BOLD signal in schizophrenic patients: anomalies in the default network. Schizophr Bull 33:1004–1012.

Chang LC, Jones DK, Pierpaoli C (2005): RESTORE: robust estimation of tensors by outlier rejection. Magn Reson Med 53:1088–1095.

Collins DL, Neelin P, Peters TM, Evans AC (1994): Automatic 3D intersubject registration of MR volumetric data in standardized Talairach space. J Comput Assist Tomogr 18:192–205.

Cordes D, Haughton VM, Arfanakis K, Wendt GJ, Turski PA, Moritz CH, Quigley MA, Meyerand ME (2000): Mapping functionally related regions of brain with functional connectivity MR imaging. AJNR Am J Neuroradiol 21:1636–1644.

Cordes D, Haughton VM, Arfanakis K, Carew JD, Turski PA, Moritz CH, Quigley MA, Meyerand ME (2001): Frequencies contributing to functional connectivity in the cerebral cortex in "resting-state" data. AJNR Am J Neuroradiol 22:1326–1333.

Damoiseaux JS, Rombouts SA, Barkhof F, Scheltens P, Stam CJ, Smith SM, Beckmann CF (2006): Consistent resting-state networks across healthy subjects. Proc Natl Acad Sci U S A 103:13848–13853.

Damoiseaux JS, Beckmann CF, Arigita EJ, Barkhof F, Scheltens P, Stam CJ, Smith SM, Rombouts SA (2008): Reduced resting-state brain activity in the "default network" in normal aging. Cereb Cortex 18:1856–1864. Epub 2007 Dec 5.

De Luca M, Beckmann CF, De Stefano N, Matthews PM, Smith SM (2006): fMRI resting state networks define distinct modes of long-distance interactions in the human brain. Neuroimage 29:1359–1367.

Dosenbach NU, Fair DA, Miezin FM, Cohen AL, Wenger KK, Dosenbach RA, Fox MD, Snyder AZ, Vincent JL, Raichle ME Schlaggar BL, Petersen SE (2007): Distinct brain networks for adaptive and stable task control in humans. Proc Natl Acad Sci U S A 104:11073–11078.

Fox MD, Raichle ME (2007): Spontaneous fluctuations in brain activity observed with functional magnetic resonance imaging. Nat Rev Neurosci 8:700–711.

Friston KJ, Frith CD, Liddle PF, Frackowiak RS (1993): Functional connectivity: The principal-component analysis of large (PET) data sets. J Cereb Blood Flow Metab 13:5–14.

Greicius MD, Krasnow B, Reiss AL, Menon V (2003): Functional connectivity in the resting brain: A network analysis of the default mode hypothesis. Proc Natl Acad Sci U S A 100:253–258.

Greicius MD, Supekar K, Menon V, Dougherty RF (2009): Resting-state functional connectivity reflects structural connectivity in the default mode network. Cereb Cortex 19:72–78. Epub 2009 Apr 9.

Gusnard DA, Raichle ME, Raichle ME (2001): Searching for a baseline: Functional imaging and the resting human brain. Nat Rev Neurosci 2:685–694.

Hagmann P, Kurant M, Gigandet X, Thiran P, Wedeen VJ, Meuli R, Thiran JP (2007): Mapping human whole-brain structural networks with diffusion MRI. PLoS ONE 2:e597.

Hagmann P, Cammoun L, Gigandet X, Meuli R, Honey CJ, Wedeen VJ, Sporns O (2008): Mapping the structural core of human cerebral cortex. PLoS Biol 6:e159.

Hulshoff Pol HE, Kahn RS (2008): What happens after the first episode? A review of progressive brain changes in chronically ill patients with schizophrenia. Schizophr Bull 34:354–366.

Hulshoff Pol HE, Schnack HG, Mandl RC, van Haren NE, Koning H, Collins DL, Evans AC, Kahn RS (2001): Focal gray matter density changes in schizophrenia. Arch Gen Psychiatry 58:1118–1125.

Hulshoff Pol HE, Schnack HG, Mandl RC, Cahn W, Collins DL, Evans AC, Kahn RS (2004): Focal white matter density changes in schizophrenia: Reduced inter-hemispheric connectivity. Neuroimage 21:27–35.

Johnston JM, Vaishnavi SN, Smyth MD, Zhang D, He BJ, Zempel JM, Shimony JS, Snyder AZ, Raichle ME (2008): Loss of resting interhemispheric functional connectivity after complete section of the corpus callosum. J Neurosci 28:6453–6458.

Jones DK (2004): The effect of gradient sampling schemes on measures derived from diffusion tensor MRI: A Monte Carlo study. Magn Reson Med 51:807–815.

Jones DK (2008): Studying connections in the living human brain with diffusion MRI. Cortex 44:936–952.

Jones DK, Horsfield MA, Simmons A (1999): Optimal strategies for measuring diffusion in anisotropic systems by magnetic resonance imaging. Magn Reson Med 42:515–525.

Koch MA, Norris DG, Hund-Georgiadis M (2002): An investigation of functional and anatomical connectivity using magnetic resonance imaging. Neuroimage 16:241–250.

Kubicki M, Park H, Westin CF, Nestor PG, Mulkern RV, Maier SE, Niznikiewicz M, Connor EE, Levitt JJ, Frumin M, Kikinis R, Jolesz FA, McCarley RW, Shenton ME (2005): DTI and MTR abnormalities in schizophrenia: Analysis of white matter integrity. Neuroimage 26,1109–1118.

Kubicki M, McCarley R, Westin CF, Park HJ, Maier S, Kikinis R, Jolesz FA, Shenton ME (2007): A review of diffusion tensor imaging studies in schizophrenia. J Psychiatr Res 41:15–30.

Latora V, Marchiori M (2001): Efficient behavior of small-world networks. Phys Rev Lett 87:198701.

Liang M, Zhou Y, Jiang T, Liu Z, Tian L, Liu H, Hao Y (2006): Widespread functional disconnectivity in schizophrenia with resting-state functional magnetic resonance imaging. Neuroreport 17:209–213.

Liu H, Liu Z, Liang M, Hao Y, Tan L, Kuang F, Yi Y, Xu L, Jiang T (2006): Decreased regional homogeneity in schizophrenia: A resting state functional magnetic resonance imaging study. Neuroreport 17:19–22.

Liu Y, Liang M, Zhou Y, He Y, Hao Y, Song M, Yu C, Liu H, Liu Z, Jiang T (2008): Disrupted small-world networks in schizophrenia. Brain 131:945.

Lowe MJ, Mock BJ, Sorenson JA. (1996): Resting state fMRI signal correlations in multi-slice EPI. Neuroimage 3(S257).

Lowe MJ, Mock BJ, Sorenson JA (1998): Functional connectivity in single and multislice echoplanar imaging using resting-state fluctuations. Neuroimage 7:119–132.

Lowe MJ, Dzemidzic M, Lurito JT, Mathews VP, Phillips MD (2000): Correlations in low-frequency BOLD fluctuations reflect cortico-cortical connections. Neuroimage 12:582–587.

Lowe MJ, Beall EB, Sakaie KE, Koenig KA, Stone L, Marrie RA, Phillips MD (2008): Resting state sensorimotor functional connectivity in multiple sclerosis inversely correlates with transcallosal motor pathway transverse diffusivity. Hum Brain Mapp 29:818–827.

Makris N, Papadimitriou GM, van der Kouwe A, Kennedy DN, Hodge SM, Dale AM, Benner T, Wald LL, Wu O, Tuch DS, Caviness VS, Moore TL, Killiany RJ, Moss MB, Rosene DL (2007): Frontal connections and cognitive changes in normal aging rhesus monkeys: A DTI study. Neurobiol Aging 28:1556–1567.

Mason MF, Norton MI, Van Horn JD, Wegner DM, Grafton ST, Macrae CN (2007): Wandering minds: The default network and stimulus-independent thought. Science 315:393–395.

Micheloyannis S, Pachou E, Stam CJ, Breakspear M, Bitsios P, Vourkas M, Erimaki S, Zervakis M (2006): Small-world networks and disturbed functional connectivity in schizophrenia. Schizophr Res 87:60–66.

Mori S, van Zijl PC (2002): Fiber tracking: Principles and strategies—A technical review. NMR Biomed 15:468–480.

Mori S, Crain BJ, Chacko VP, van Zijl PC (1999): Three-dimensional tracking of axonal projections in the brain by magnetic resonance imaging. Ann Neurol 45:265–269.

Mori S, Kaufmann WE, Davatzikos C, Stieltjes B, Amodei L, Fredericksen K, Pearlson GD, Melhem ER, Solaiyappan M, Raymond GV, Moser HW, van Zijl PC (2002): Imaging cortical association tracts in the human brain using diffusion-tensor-based axonal tracking. Magn Reson Med 47:215–223.

Nestor PG, Kubicki M, Spencer KM, Niznikiewicz M, McCarley RW, Shenton ME (2007): Attentional networks and cingulum bundle in chronic schizophrenia. Schizophr Res 90:308–315.

Nir Y, Mukamel R, Dinstein I, Privman E, Harel M, Fisch L, Gelbard-Sagiv H, Kipervasser S, Andelman F, Neufeld MY Kramer U, Arieli A, Fried I, Malach R (2008): Interhemispheric correlations of slow spontaneous neuronal fluctuations revealed in human sensory cortex. Nat Neurosci 11:8.

Raichle ME, MacLeod AM, Snyder AZ, Powers WJ, Gusnard DA, Shulman GL (2001): A default mode of brain function. Proc Natl Acad Sci U S A 98:676–682.

Raichle ME, Snyder AZ (2007): A default mode of brain function: A brief history of an evolving idea. Neuroimage 37:1083–1090.

Salvador R, Suckling J, Coleman MR, Pickard JD, Menon D, Bullmore E (2005a): Neurophysiological architecture of functional magnetic resonance images of human brain. Cereb Cortex 15:1332–1342.

Salvador R, Suckling J, Schwarzbauer C, Bullmore E (2005b): Undirected graphs of frequency-dependent functional connectivity in whole brain networks. Philos Trans R Soc Lond B Biol Sci 360:937–946.

Salvador R, Martinez A, Pomarol-Clotet E, Sarro S, Suckling J, Bullmore E (2007): Frequency based mutual information measures between clusters of brain regions in functional magnetic resonance imaging. Neuroimage 35:83–88.

Schmahmann JD, Pandya DN (2006): Fiber Pathways of the Brain. New York: Oxford University Press. pp 485–496.

Schmahmann JD, Pandya DN, Wang R, Dai G, D'Arceuil HE, de Crespigny AJ, Wedeen VJ (2007): Association fibre pathways of the brain: Parallel observations from diffusion spectrum imaging and autoradiography. Brain 130 (Part 3):630–653.

Schneiderman JS, Buchsbaum MS, Haznedar MM, Hazlett EA, Brickman AM, Shihabuddin L, Brand JG, Torosjan Y, Newmark RE, Tang C, Aronowitz J, Paul-Odouard R, Byne W, Hof PR (2007): Diffusion tensor anisotropy in adolescents and adults. Neuropsychobiology 55:96–111.

Seeley WW, Menon V, Schatzberg AF, Keller J, Glover GH, Kenna H, Reiss AL, Greicius MD (2007): Dissociable intrinsic connectivity networks for salience processing and executive control. J Neurosci 27:2349–56.

Shi J, Malik J (2000): Normalized cuts and image segmentation. IEEE Trans on pattern analysis and machine intelligence 22:17.

Shmuel A, Leopold DA (2008): Neuronal correlates of spontaneous fluctuations in fMRI signals in monkey visual cortex: Implications for functional connectivity at rest. Hum Brain Mapp 29:751–761.

Shmueli K, van Gelderen P, de Zwart JA, Horovitz SG, Fukunaga M, Jansma JM, Duyn JH (2007): Low-frequency fluctuations in the cardiac rate as a source of variance in the resting-state fMRI BOLD signal. Neuroimage 38:306–320.

Sridharan D, Levitin DJ, Menon V (2008): A critical role for the right fronto-insular cortex in switching between central-executive and default-mode networks. Proc Natl Acad Sci U S A 105:12569–12574.

Stam CJ (2004): Functional connectivity patterns of human magnetoencephalographic recordings: A 'small-world' network? Neurosci Lett 355:25–28.

Stam CJ, Jones BF, Nolte G, Breakspear M, Scheltens P (2007): Small-world networks and functional connectivity in Alzheimer's disease. Cereb Cortex 17:92–99.

Sun Z, Wang F, Cui L, Breeze J, Du X, Wang X, Cong Z, Zhang H, Li B, Hong N, Zhang D (2003): Abnormal anterior cingulum in patients with schizophrenia: A diffusion tensor imaging study. Neuroreport 14:1833–1836.

Van den Heuvel MP, Mandl RC, Hulshoff Pol HE (2008a): Normalized group clustering of resting-state fMRI data. PLoS ONE 3:e2001.

Van den Heuvel MP, Mandl RC, Luigjes J, Hulshoff Pol HE (2008b): Microstructural organization of the cingulum tract and the level of default mode functional connectivity. J Neurosci 28:10844–10851.

Van den Heuvel MP, Stam CJ, Boersma M, Hulshoff Pol HE (2008c): Small-world and scale-free organization of voxel based resting-state functional connectivity in the human brain. Neuroimage 43:528–539.

Vincent JL, Kahn I, Snyder AZ, Raichle ME, Buckner RL (2008): Evidence for a frontoparietal control system revealed by intrinsic functional connectivity. J Neurophysiol 100:3328–3342.

Vogt BA, Pandya DN (1987): Cingulate cortex of the rhesus monkey: II. Cortical afferents. J Comp Neurol 262:271–289.

Wakana S, Jiang H, Nagae-Poetscher LM, van Zijl PC, Mori S (2004): Fiber tract-based atlas of human white matter anatomy. Radiology 230:77–87.

Watts DJ, Strogatz SH (1998): Collective dynamics of 'small-world' networks. Nature 393:440–442.

Wise RG, Ide K, Poulin MJ, Tracey I (2004): Resting fluctuations in arterial carbon dioxide induce significant low frequency variations in BOLD signal. Neuroimage 21:1652–1664.

Xiong J, Parsons LM, Gao JH, Fox PT (1999): Interregional connectivity to primary motor cortex revealed using MRI resting state images. Hum Brain Mapp 8:151–156.

Yoon B, Shim YS, Lee KS, Shon YM, Yang DW. (2007): Region-specific changes of cerebral white matter during normal aging: A diffusion-tensor analysis. Arch Gerontol Geriatr 47: 129–138.

Zhang D, Snyder AZ, Fox MD, Sansbury MW, Shimony JS, Raichle ME (2008): Intrinsic functional relations between human cerebral cortex and thalamus. J Neurophysiol 100:1740–1748.